Application of RTDF to particles with curved surfaces

E. Hesse*, D.S. Mc Call, Z. Ulanowski, C. Stopford, and P.H. Kaye

University of Hertfordshire, Centre for Atmospheric and Instrumentation Research, Hatfield, Hertfordshire, AL10 9AB, UK

Abstract

The applicability of the Ray Tracing with Diffraction on Facets model is extended to particles with curved surfaces. This allows tests against *T*-matrix calculations for larger size parameters and modeling of light scattering by more realistic particle shapes, such as ice crystals with rounded edges.

* Tel.: 441707286170; fax: +44 1707 284185.
E-mail address: e.hesse@herts.ac.uk

1 Introduction

The importance of ice and mixed-phase clouds to the earth-atmosphere radiation balance and climate is well established. However, despite extensive study, there is still a large uncertainty over the radiative properties of these clouds. This is partly due to inadequate theoretical models of light scattering by the constituent ice crystals of realistic shapes and sizes.

Computations of light scattering properties for non-spheroidal particles based on exact methods like the Separation of Variables (SVM) Method, e.g. [1], *T*-matrix [2,3], Discrete Dipole Approximation (DDA) [4] have upper size parameter limits of applicability, depending on the method and the complexity of particle shape. This leaves a size parameter range that is covered neither by exact methods nor by Geometric Optics (GO). A modified Kirchhoff approximation (MKA) method has been introduced [5] to calculate far fields from classical Geometric Optics (GO) results, which encouraged the development of the Improved GO model [6]. The latter is, however, computationally expensive. For moderate values of the size parameter the Finite Difference Time Domain (FDTD) method can be used [7] but it too, puts severe demands on computational resources. Thus, despite its limitations, Geometric Optics (GO) combined with projected-area diffraction, e.g. [8], is still the most widely used model for moderate to large size parameters. Recently, diffraction on facets was introduced into a ray tracing model (Ray Tracing with Diffraction on Facets, RTDF) [9-11]. This method maintains the flexibility and computational efficiency of GO while producing much improved results. Given the rapid and flexible computation offered by ray-tracing based models, it is possible to create two-dimensional (2D) light scattering patterns for even very complex crystals. Such patterns provide much more information than azimuthally averaged scattering data such as a phase function. In contrast to standard GO, the RTDF model can produce such patterns not only for random (averaged) orientations but also for fixed ones. 2D scattering patterns have been correctly predicted by the RTDF model [10], and it is therefore expected to become a suitable tool for particle characterization, in particular since cloud probes now exist that characterize ice particles on the basis of 2D scattering patterns (e.g. [12]). A large proportion of ice crystals have curved as well as planar surface components, e.g. due to sublimation or melting. Other atmospheric particles, like mineral dust, are irregular. Their surfaces could be approximated as multifaceted objects. In this paper, the RTDF model is used to model scattering by 'hybrid' particles, the surface of which has both planar and

curved components. RTDF phase functions of circular cylinders and a sphere are compared with *T*-matrix [13] or Mie theory, which are analytical techniques, and GO combined with projected area diffraction [8]. The effect of edge rounding on 2D scattering patterns of hexagonal columns is demonstrated.

2 Method and results

The RTDF model combines ray tracing with diffraction on flat facets. The model calculates diffraction using an approximation for the far-field direction of the Poynting vector. The angle of diffraction of a reflected or refracted ray is calculated from the ray's proximity to the facet edges [11]. In the following, curved surfaces will be approximated by arrays of planar facets. As an example, the lateral surface of a circular cylinder will be approximated by a succession of thin strips. The approximation of a curved surface will improve with the number of plane facet elements, avoiding artificial sharp edges and therefore reducing artefact structures in the angular distribution of scattered light. Furthermore, a decrease of the angle between surface normals of neighbouring facets needs to be accompanied by a reduction of diffraction at these facets. In the following, the far field deflection angle φ_o calculated by RTDF [11] is multiplied by the sine of the angle γ between the normals of the neighbouring facets under consideration, if $\gamma < 90°$:

$$\varphi = \varphi_o \sin\gamma \quad \forall\ 0 < \gamma < \pi/2$$
$$\varphi = \varphi_o \quad \forall\ \pi/2 < \gamma < \pi$$

This ensures that no diffraction takes place between coplanar facets. Full far field diffraction is applied between facets with normals which include an angle of 90° or larger. The ray-tracing component and the diffraction on projected cross section component are added, as in the original ray-tracing code by Macke [8]. Calculations for diffraction at circular apertures showed however, that the existing subroutine for diffraction at polygonal apertures generates too high scattering contributions close to the forward direction for size parameters $2\pi a/\lambda$ smaller than about 100 (a is the effective radius of the aperture). This is because a singularity of the diffraction formula at direct forward scattering is approached. Therefore, in this work the projected cross section is approximated by a circular aperture of the same area, which should be adequate for particles with aspect ratios close to one, such as those investigated here. The RTDF results are compared with computations using *T*-matrix [13,14] or

Mie theory, respectively, which are analytical techniques, and GO combined with projected area diffraction [8]. For the GO calculations the same approximation for the projected cross sections as for RTDF was used.

Fig. 1 shows randomized orientation phase functions for a circular cylinder with refractive index 1.311 for size parameters $x = 2\pi a_{sph}/\lambda$ equal to 20, 40, 80 and 120, where a_{sph} is the radius of a sphere with equivalent surface area. The aspect ratio of the column $L/2a$ is 1, where L is the column length and $2a$ its diameter. Down to size parameters of about 20 the RTDF results approximate the *T*-matrix calculations much better than GO over the whole angular range, and in particular in near exact forward and backscattering, in the halo region, and in the backscattering region. In agreement with the *T*-matrix calculations [13], the RTDF results show that size parameter 40 is too small to produce a pronounced 46° halo. Diffraction features appear slightly wider in RTDF than in the *T*-matrix results due to the approximation of diffraction during internal reflection and refraction steps by far field values (multiplied by sin γ according to eq.(1)), currently implemented in the RTDF model [11].

Fig. 2 shows asymmetry parameters vs. size parameters as calculated by the *T*-matrix method, RTDF and GO. The *T*-matrix values oscillate between 0.738 and 0.797 due to interference effects which are currently not included in RTDF. The oscillation amplitude decreases and the average value of the envelopes (also shown in the graph) increases with size parameter. RTDF and GO-values are higher than the *T*-matrix average over the whole investigated range and increase with size parameter, too. For GO this increase is entirely due to reduced diffraction on the projected cross section area. The RTDF values are lower than those of GO and approach the latter at high size parameters, where little diffraction takes place at facets. RTDF is a better fit to the *T*-matrix values than GO, however a nearly constant difference between RTDF and *T*-matrix of about 0.009 over the whole investigated range remains. One should note that in general the asymmetry parameter is dominated by the comparatively high intensity in near forward scattering, but is less influenced by scattering features like halos occurring within lower intensity regions at higher scattering angles and therefore does not reflect the improvement of RTDF over GO in these regions. Scattering features away from the forward scattering peak can be detected by multi-angle measurements, e.g. using nephelometers [12] and can be used to classify particles (see below).

Fig. 3 shows the phase function of a sphere of size parameter 50 (n=1.33) calculated by Mie theory using the code by Mishchenko et al. [15]. For RTDF and GO calculations the sphere was

approximated by 800, 1352 and 2592 facets (corresponding to 9°, 7° and 5° angles between normals of adjacent facets, respectively). Apart from six triangular facets connecting at each of the poles, all facets are trapezoidal. As is well known, the GO phase function of a perfect sphere shows the primary and secondary rainbow peak separated by Alexander's dark band (see e.g. [16]). Approximating a sphere by a facetted object has the effect of widening and merging the rainbow peaks, which are angles of minimum and maximum deviation. As to be expected, RTDF calculations result in even wider rainbow features. If the number of facets is large enough, RTDF results in a better approximation of the *T*-matrix result than GO, as can be seen in the example calculation for 2592 facets. The shown comparisons of phase functions of cylinders and a sphere calculated by *T*-matrix and RTDF demonstrate the suitability of RTDF for modelling phase functions of particles of complex shape, for example crystals with rounded edges or mineral dust grains.

As mentioned above, RTDF can be used to calculate 2D scattering patterns. Fig. 4a shows such patterns calculated for a hexagonal column of size parameter $2\pi a/\lambda$, where a is the edge length of the basal facet, aspect ratio $L/2a=3$ and orientation described by Euler angles $\alpha=0°$, $ß=70°$, $\gamma=10°$, as seen from the perspective of the incident beam. Fig. 4b shows the pattern for the same column but with rounded long edges of the prism facets. The circumscribing circle has a radius of $0.956a$. Rounded edges are approximated by a succession of eight thin facets, each of which covers an angular segment of 1° around the long axis of the column.

The main feature in both scattering patterns is the bright arc through forward scattering. In Fig. 4a three bright spots are situated on the arc. The central one is essentially due to rays entering through facet 4 and leaving through facet 7 (see Fig. 4a for facet numbers). The two outer ones are due to refraction through 60° prisms, entering through facets 5 and 3 respectively, and leaving through facet 7. The additional bright spots along the arc in Fig. 4b are due to rays passing through edge facets. The double features left and right of the central bright spot are due to rays entering through facet 4 and leaving through the (rounded) edge between facets 6 and 7, and rays entering at the edge between facets 3 and 4 and leaving through facet 7, respectively. The splitting of these spots is due to the approximation of the curved edge by a discrete number of plane facets. In Figs. 4a and b, the central spot on the arc is connected to one bright spot almost directly above, corresponding to refraction through facets 1 and 7. In Fig 4b, an additional bright spot slightly to the left of the previous one is due to rays refracted through facet 1 and the edge between facets 6 and 7. Below

each of the three maxima on the arc in Fig. 4a is another spot due to more complicated ray paths entering through facet 5, 4, and 3, respectively. (The central lower spot is stronger than the outer ones due to contributions by external reflection from facet 1.) In Fig. 4b spots corresponding to each additional intensity maximum along the arc caused by ray paths through edge facets can be found.

3 Conclusion

The RTDF model has been developed further to approximate curved surfaces by an array of planar facets and taking into account the angle between surface normals when calculating diffraction during ray-tracing. The enhanced RTDF model has been tested against *T*-matrix results for circular cylinders and against Mie theory for a sphere. The RTDF results approximate the exact calculations much better than GO over the whole angular range and in particular in near-exact forward and backscattering, and in the halo region. The modification of 2D scattering patterns by rounding the edges of pristine crystals has been demonstrated for a hexagonal column. The expansion of the applicability of the RTDF model towards particles with curved surfaces and 'hybrid particles', which have plane as well as curved surfaces is potentially useful for the calculation of the scattering properties of ice crystals of realistic shapes as well as of irregular particles like mineral dust grains and comparison with experimental data.

Acknowledgment

This research was supported by the Natural Environment Research Council of the UK. The authors are grateful to A. Macke for providing the ray-tracing code and to M.I. Mishchenko for making the T-matrix code publicly available.

References

[1] Rother T, Schmidt K, Havemann S. Light scattering on hexagonal ice columns. J Opt Soc Am A 2001;18:2512-2517.

[2] Mishchenko MI, Videen G, Babenko VA, Khlebtsov NG, Wriedt T. T-matrix theory of electromagnetic scattering by particles and its applications: a comprehensive reference database. JQSRT 2004;88:357-406.

[3] Mishchenko MI, Videen G, Babenko VA, Khlebtsov NG, Wriedt T. Comprehensive T-matrix reference database: A 2004-06 update. JQSRT 2007;106:304-324.

[4] Yurkin MA, Hoekstra AG. The discrete dipole approximation: An overview and recent developments. JQSRT 2007;106:558-589.

[5] Muinonen K. Scattering of light by crystals: a modified Kirchhoff approximation. Appl Opt 1989;28:3044-3050.

[6] Yang P, Liou KN. Geometric-optics-integral equation method for light scattering by nonspherical ice crystals. Appl Opt 1996;35:6568-6584.

[7] Yang P, Liou KN. In: Mishchenko MI, Hovenier JW, Travis LD, editors. *Light scattering by nonspherical particles*, (New York: Academic Press, 1999. p. 173-221).

[8] Macke A, Mueller J, Raschke E. Single scattering properties of atmospheric ice crystals. J Atmos Sci 1996;53:2813-2825.

[9] Hesse E, Ulanowski Z. Scattering from long prisms using ray tracing combined with diffraction on facets. JQSRT 2003; 79-80C:721-732.

[10] Clarke AJM, Hesse E, Ulanowski Z and Kaye PH. A 3D implementation of ray-tracing with diffraction on facets: Verification and a potential application. JQSRT 2006;100:103-114.

[11] Hesse E. Modelling diffraction during ray-tracing using the concept of energy flow lines. JQSRT 2008;109, 1374–1383.

[12] Kaye PH, Hirst E, Greenaway RS, Ulanowski Z, Hesse E, DeMott PJ, Saunders C, Connely P. Classifying atmospheric light scattering by spatial light scattering. Opt Lett 2008;33:1545-1547.

[13] Mishchenko MI, Macke A. How big should hexagonal ice crystals be to produce halos? Appl Opt 1999;38:1626-1629.

[14] Mishchenko MI and Travis LD. Capabilities and limitations of a current FORTRAN implementation of the T-matrix method for randomly oriented, rotationally symmetric scatterers. JQSRT 1998;60:309-324.

[15] Mishchenko MI, Dlugach JM, Yanovitskij EG, Zakharova, NT. Bidirectional reflectance of flat, optically thick particulate layers: an efficient radiative transfer solution and applications to snow and soil surfaces. JQSRT 1999;63:409-432.

[16] Liou KN and Hansen JE. Intensity and polarization for single scattering by polydisperse spheres: a comparison of ray optics and Mie theory. J Atmos Sci 1971;28:995-1004.

Captions of figures

Figure 1: Randomized phase functions for circular cylinders with refractive index n = 1.311, aspect ratio $L/2a$ = 1 and size parameters $x = 2\pi a_{sph}/\lambda$ of (a) 20, (b) 40, (c) 80 and (d) 120, respectively, calculated using RTDF in comparison with *T*-matrix [13,14] and GO with projected area diffraction [8] results.

Figure 2: Asymmetry parameters vs. size parameters as calculated by the *T*-matrix method, RTDF and GO.

Figure 3: Phase function of a sphere of size parameter 50 and refractive index 1.33 calculated using Mie theory and phase functions calculated by RTDF and GO for sphere approximations with 800, 1352 and 2592 facets, respectively.

Figure 4: a) Orientation of a hexagonal column (α=0°, ß=70°, γ=10°) from the point of view of the incident light and scattering pattern projected into the forward facing hemisphere; the facets are numbered as shown. b) Schematic and scattering pattern for the same column as in Fig. a), but with rounded long edges of the prismatic faces.

Fig. 1a)

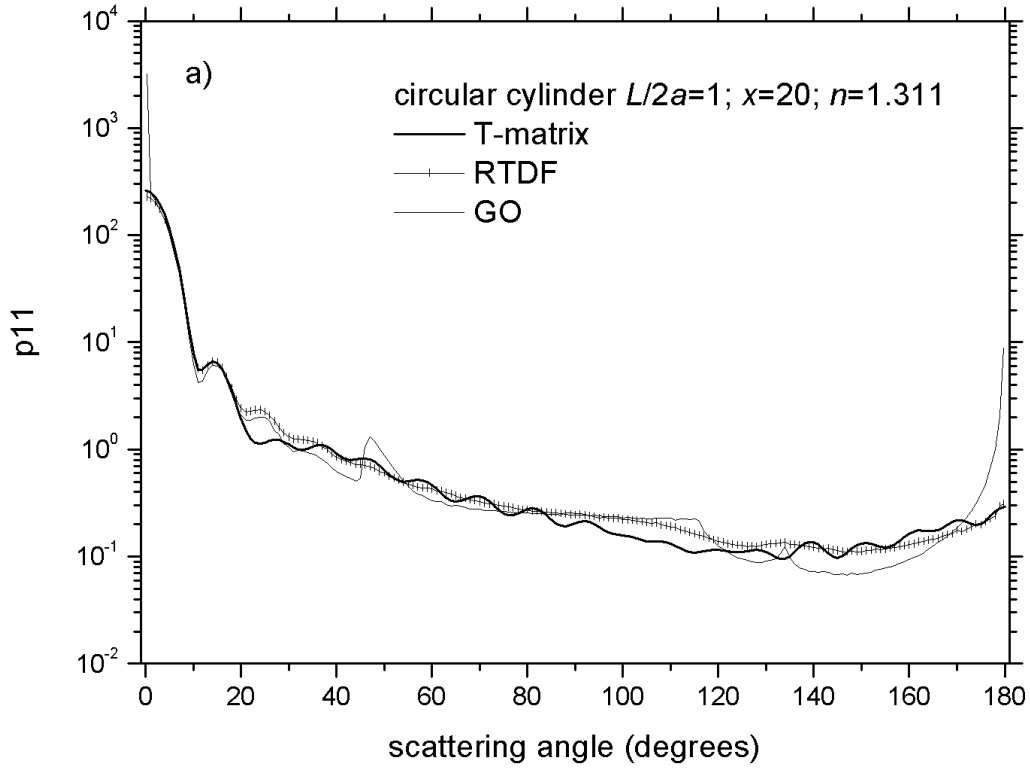
a)
circular cylinder L/2a=1; x=20; n=1.311
T-matrix
RTDF
GO
p11
scattering angle (degrees)

Fig.1b)

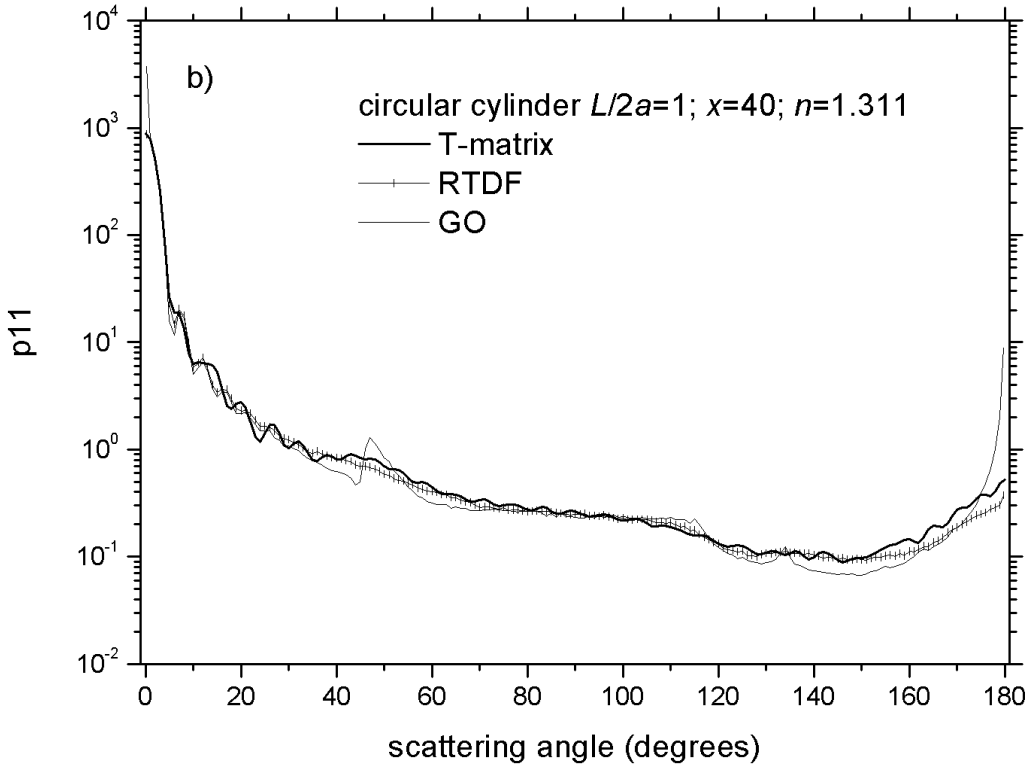
b)
circular cylinder L/2a=1; x=40; n=1.311
T-matrix
RTDF
GO
p11
scattering angle (degrees)

Fig.1c)

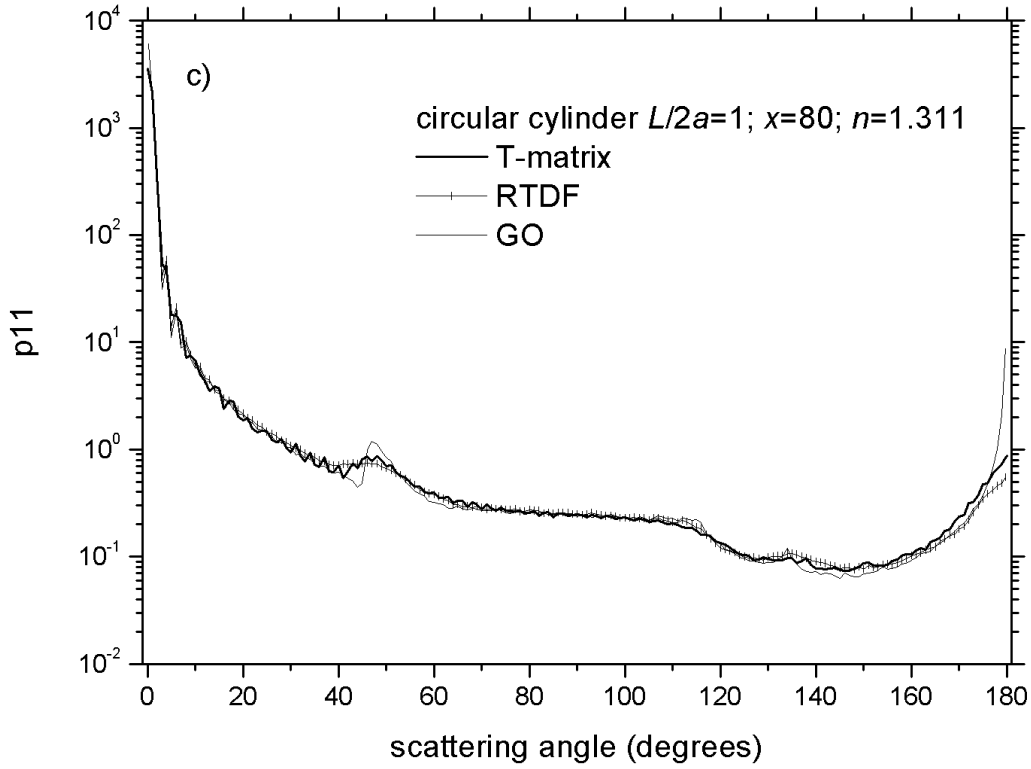
c)
circular cylinder L/2a=1; x=80; n=1.311
T-matrix
RTDF
GO
p11
scattering angle (degrees)

Fig.1d)

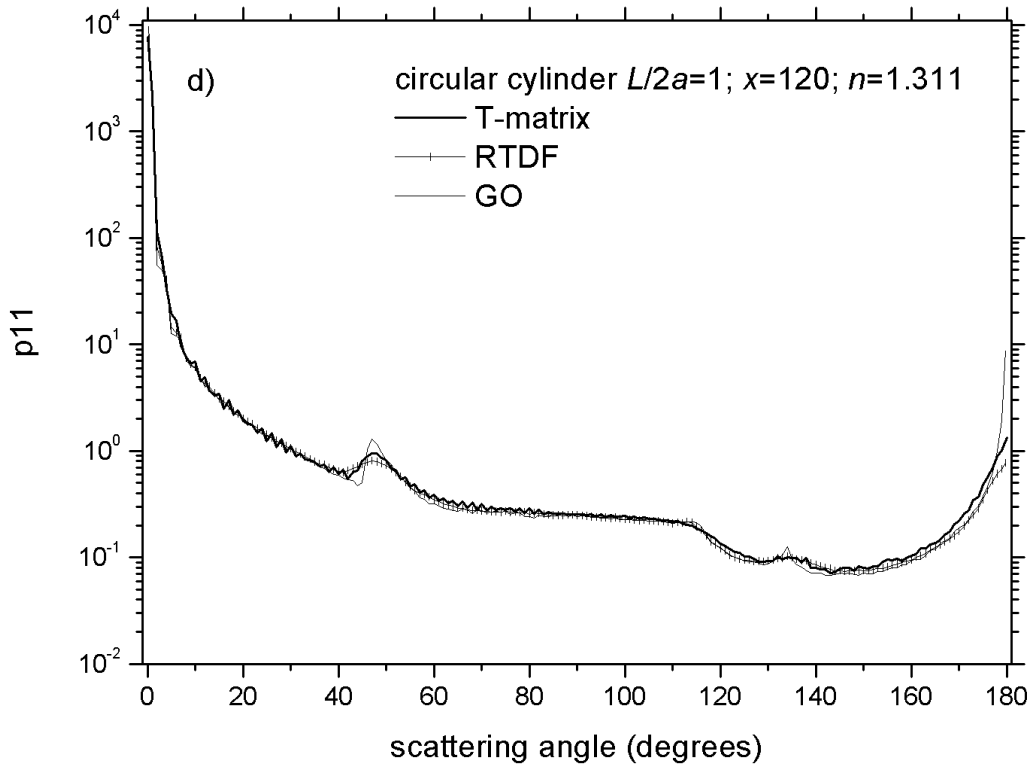
d)
circular cylinder L/2a=1; x=120; n=1.311
T-matrix
RTDF
GO
p11
scattering angle (degrees)

Fig.2

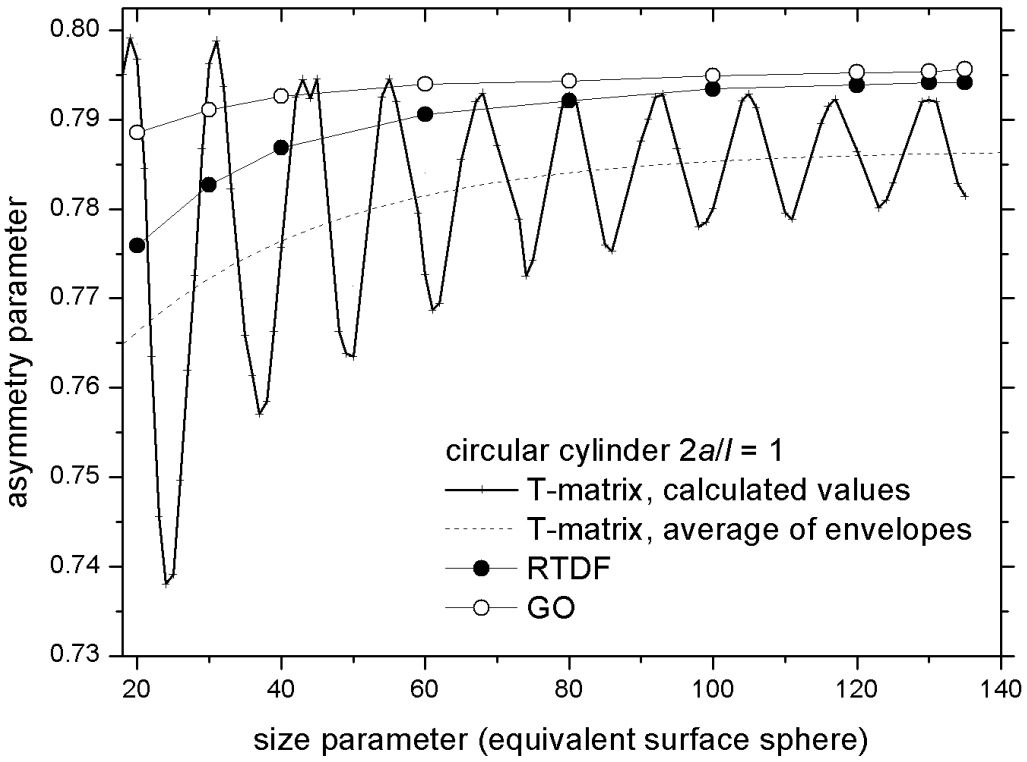
asymmetry parameter
size parameter (equivalent surface sphere)
circular cylinder 2a/l = 1
T-matrix, calculated values
T-matrix, average of envelopes
RTDF
GO

Fig.3

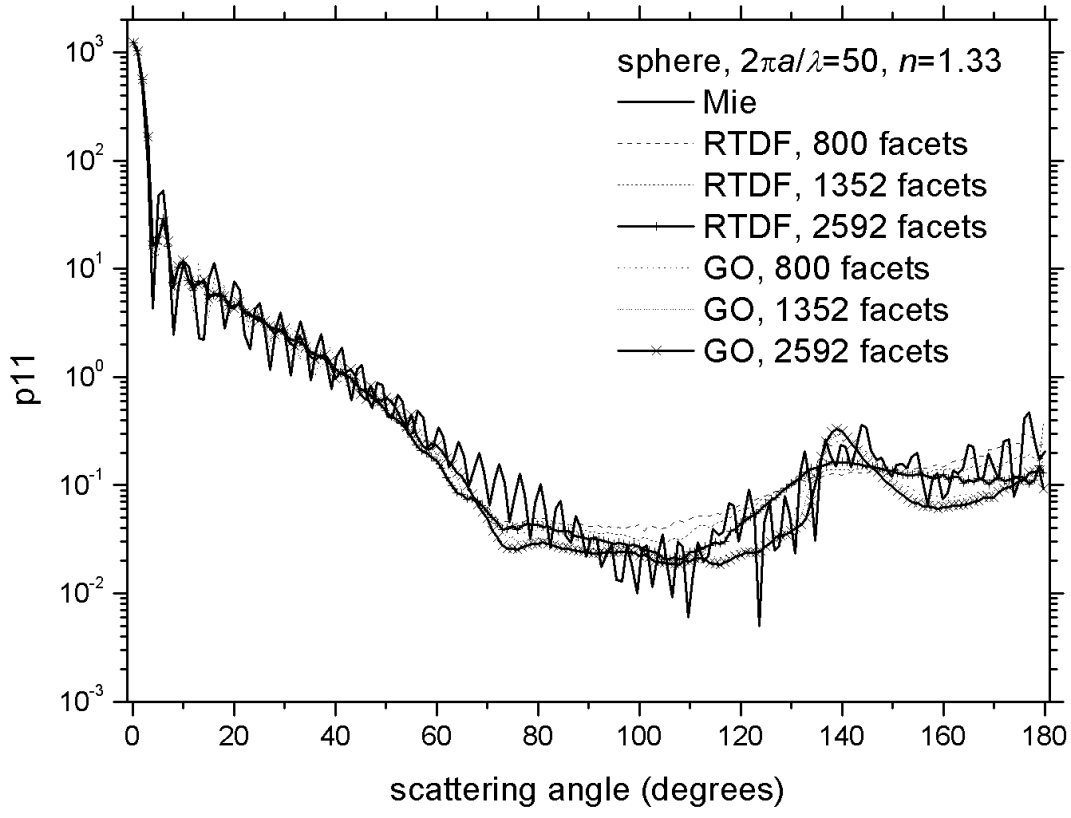
p11
scattering angle (degrees)
sphere, 2πa/λ=50, n=1.33
Mie
RTDF, 800 facets
RTDF, 1352 facets
RTDF, 2592 facets
GO, 800 facets
GO, 1352 facets
GO, 2592 facets

Fig.4

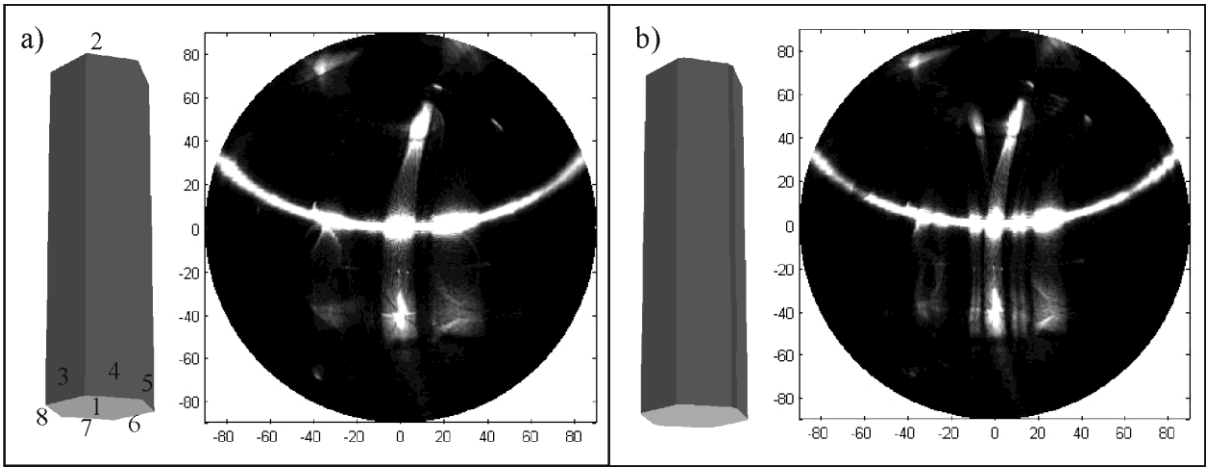
a)
2
3
4
5
8
1
7
6
80
60
40
20
0
-20
-40
-60
-80
-80 -60 -40 -20 0 20 40 60 80
b)
80
60
40
20
0
-20
-40
-60
-80
-80 -60 -40 -20 0 20 40 60 80